

Learn to Predict Equilibria via Fixed Point Networks

Howard Heaton^{*1} Daniel McKenzie^{*2} Samy Wu Fung³ Qiuwei Li⁴ Stan Osher² Wotao Yin⁴

Abstract

Systems of competing agents can often be modeled as games. Assuming rationality, the most likely outcomes are given by an *equilibrium*, e.g. a Nash equilibrium. In many practical settings, games are influenced by *context*, i.e. additional data beyond the control of any agent (e.g. weather for traffic and fiscal policy for market economies). Often only game equilibria are observed, while the players' true cost functions are unknown. This work introduces Nash Fixed Point Networks (N-FPNs), a class of implicit neural networks that learn to predict the equilibria *given only the context*. The N-FPN design fuses data-driven modeling with provided constraints on the actions available to agents. N-FPNs are compatible with the recently introduced Jacobian-Free Backpropagation technique for training implicit networks, making them significantly faster to train than prior models. N-FPNs can exploit novel constraint decoupling to avoid costly projections. Provided numerical examples show the efficacy of N-FPNs on atomic and non-atomic games (e.g. traffic routing).¹

1. Introduction

Many recent works in deep learning highlight the power of using end-to-end learning in conjunction with known analytic models and constraints (Bertsimas et al., 2015; de Avila Belbute-Peres et al., 2018; Ling et al., 2018; 2019; Li et al., 2020; Kotary et al., 2021; Chen et al., 2021). This best-of-both worlds approach fuses the flexibility of learning-based approaches with the interpretability of models derived by domain experts. We further this line of research by proposing a practical framework for learning to predict the outcomes of contextual (i.e. parametrized) games from historical data, while respecting constraints on players' actions.

^{*}Equal contribution ¹Typal Research, Typal LLC ²Department of Mathematics, UCLA ³Department of Applied Mathematics and Statistics, Colorado School of Mines ⁴AliBaba USA . Correspondence to: Daniel McKenzie <mckenzie@math.ucla.edu>.

¹Codes available at github.com/DanielMckenzie/Nash_FPNs.

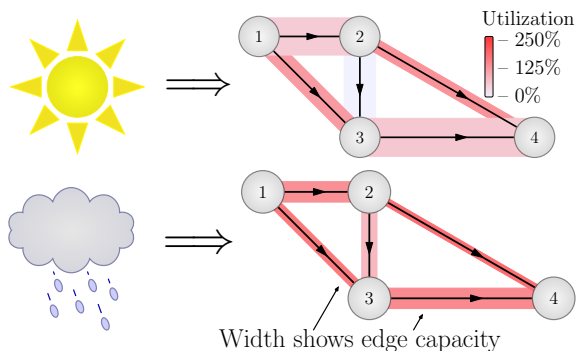


Figure 1. Proposed N-FPNs can predict traffic flow given contextual information (e.g. weather), e.g. road capacities reduce on rainy days and light/dark red edges show light/heavy traffic.

Many social systems can aptly be analyzed as games, including market economies (Arrow & Debreu, 1954), traffic routing (Wardrop, 1952), even penalty kicks in soccer (Azar & Bar-Eli, 2011). We consider games with costs parametrized by a context variable d , beyond the control of any player. As in the multi-armed bandit literature, we call such games *contextual* (Sessa et al., 2020). For example, in traffic routing, d may encode factors like weather, local sporting events or tolls influencing drivers' commutes.

Game-theoretic analyses frequently assume players' cost functions are known *a priori* and seek to predict how players will act, typically by computing a Nash equilibrium x_d^* (Nash, 1950). Informally, a Nash equilibrium is a choice of strategy for each player such that no player can improve their outcomes via unilateral deviation. However, in practice the cost functions are frequently unknown. Here, we consider the problem of predicting equilibria, *given only contextual information*, without knowing players' cost functions.

For non-contextual games, many prior works (see Section 4) seek to use (noisy) observations of the Nash equilibrium to learn the cost functions. Our approach is different. We propose a new framework: Nash Fixed Point Networks (N-FPNs). Each N-FPN is trained on historical data pairs (d, x_d^*) to "predict the appropriate game from context and then output game equilibria" by defining a tunable operator with fixed points that coincide with Nash equilibria. N-FPN inferences are computed by repeated application of the operator until a fixed point condition is satisfied. Thus, by con-

struction, N-FPNs are implicit networks — neural networks evaluated using an arbitrary number of layers (Winston & Kolter, 2020; Bai et al., 2019; Ghaoui et al., 2019; Fung et al., 2022) — and the operator weights can be efficiently trained using Jacobian-free backpropagation (Fung et al., 2022). N-FPNs use a decoupling scheme to avoid direct, costly projections onto sets of constraints for players’ actions — the computational bottleneck of prior works (Ling et al., 2018; 2019; Li et al., 2020). For a certain class of games, we show N-FPNs have universal expressive capacity. Our framework applies equally to atomic games (*i.e.* the set of players is finite) and certain non-atomic games, particularly traffic routing (Roughgarden, 2007).

Contributions We provide a *scalable* data-driven framework for efficiently predicting equilibria in systems modeled as contextual games. Specifically, we do the following.

- ▶ Provide a general, expressible, and end-to-end trained N-FPN design that outputs Nash equilibria.
- ▶ Present a scheme for decoupling constraints, giving efficient forward and backward propagation.
- ▶ Demonstrate empirically the scalability of N-FPNs to large-scale problems.
- ▶ Create a contextual traffic routing benchmark dataset.

2. Preliminaries

We begin with a brief review of relevant game theory. After establishing notation, we provide a set of assumptions under which the mapping $d \mapsto x_d^*$ is “well-behaved.” We then describe variational inequalities and how Nash equilibria can be characterized using fixed point equations.

2.1. Games and Equilibria

Let \mathcal{X} be a finite dimensional Hilbert space. A K -player normal form contextual game is defined by action sets² \mathcal{V}_k and cost functions $u_k : \mathcal{X} \times \mathcal{D} \rightarrow \mathbb{R}$ for $k \in [K]$, where the constraint profile is $\mathcal{C} \triangleq \mathcal{V}_1 \times \dots \times \mathcal{V}_K$ and \mathcal{D} denotes the set of contexts (*i.e.* data space). The k -th player’s action x_k is constrained to the action set \mathcal{V}_k , yielding an action profile $x = (x_1, \dots, x_K) \in \mathcal{C} \subseteq \mathcal{X}$. Actions of all players other than k are $x_{-k} = (x_1, \dots, x_{k-1}, x_{k+1}, \dots, x_K)$. Each rational player aims to minimize their cost function u_k by controlling only x_k while explicitly knowing u_k is impacted by other players’ actions x_{-k} . An action profile x_d^* is a *Nash equilibrium* (NE) provided, for all $x_k \in \mathcal{V}_k$ and $k \in [K]$,

$$u_k(x_k, x_{d,-k}^*) \geq u_k(x_{d,k}^*, x_{d,-k}^*). \quad (1)$$

²These are also known as *decision sets* and/or *strategy sets*.

In words, x_d^* is a Nash equilibrium if no player can decrease their cost by unilaterally deviating from x_d^* .

We assume the following:

- (A1) $\mathcal{C} \subseteq \mathcal{X}$ is closed and convex.
- (A2) The cost functions $u_k(x; d)$ are continuously differentiable with respect to x .
- (A3) For all x , each $\nabla_x u_k(x; \cdot)$ is Lipschitz.
- (A4) Each cost function $u_k(x_k, x_{-k}; d)$ is α -strongly convex with respect to x_k .
- (A5) The set of contextual data \mathcal{D} is compact.

The assumptions yield well-behaved Nash equilibria.

Theorem 2.1. *If Assumptions (A1) to (A5) hold, then*

- (1) *there is a unique Nash Equilibrium x_d^* for all $d \in \mathcal{D}$;*
- (2) *the map $d \mapsto x_d^*$ is Lipschitz continuous.*

If (A4) holds, we define the *game gradient* by

$$F(x; d) \triangleq [\nabla_{x_1} u_1(x; d)^\top \dots \nabla_{x_K} u_K(x; d)^\top]^\top. \quad (2)$$

Remark 2.2. (A4) is fairly restrictive, but is in line with prior work (Ling et al., 2018; Li et al., 2020; Allen et al., 2021; Bertsimas et al., 2015; Ratliff et al., 2014; Zhang & Paschalidis, 2017; Zhang et al., 2018). We suspect a “local strict convexity” assumption suffices if one fixes the N-FPN iteration initialization (as done in our experiments).

2.2. Variational Inequalities

This subsection briefly outlines variational inequalities and their connection to games. Throughout this work, all sets \mathcal{C} are assumed to be closed, convex and nonempty.

Definition 2.3. For $\alpha > 0$ and $d \in \mathcal{D}$, a mapping $F : \mathcal{X} \times \mathcal{D} \rightarrow \mathcal{X}$ is α -*cocoercive*³ provided, for all $x, y \in \mathcal{X}$,

$$\langle F(x; d) - F(y; d), x - y \rangle \geq \alpha \|F(x; d) - F(y; d)\|^2. \quad (3)$$

If (3) holds upon taking $\alpha = 0$, then $F(\cdot; d)$ is *monotone*.

Definition 2.4. Given $d \in \mathcal{D}$, a point $x_d^* \in \mathcal{C}$ is a *variational inequality (VI) solution* provided

$$\langle F(x_d^*; d), x - x_d^* \rangle \geq 0, \quad \text{for all } x \in \mathcal{C}. \quad (\text{VI})$$

The solution set for (VI) is denoted by $\text{VI}(F(\cdot; d), \mathcal{C})$.

Nash equilibria may be characterized using VIs (Facchinei & Pang, 2007); namely,

$$x_d^* \text{ is an NE} \iff x_d^* \in \text{VI}(F(\cdot; d), \mathcal{C}). \quad (4)$$

That is, x_d^* is an NE if no unilateral change improves any single cost and a VI solution if no feasible update improves the sum of all costs. By (4), these views are equivalent.

³This is also known as α -inverse strongly monotone

Attribute	Analytic	Feedforward	Ling et al. (2018); Li et al. (2020)	Proposed N-FPNs
Output is Equilibria	✓		✓	✓
Data-Driven		✓	✓	✓
Constraint Decoupling	✓			✓
Simple Backprop	NA	✓		✓

Table 1. Comparison of different equilibria prediction methods. Analytic modeling algorithms yield game equilibria that are not data-driven. Traditional feed-forward networks are data-driven and easy to train, but are incapable of outputting a game equilibrium. Existing game-based implicit models are nontrivial to train (backpropagate) and require intricate forward propagation.

2.3. Implicit Neural Networks

Commonplace feedforward neural networks are a composition of parametrized functions $T_{\Theta}^{\ell}(\cdot)$ (called layers) which take data d as input and return a prediction y . Formally, given d , a network \mathcal{N}_{Θ} computes each inference y via

$$y = \mathcal{N}_{\Theta}(x) = x^{L+1}, \quad (5)$$

where $x^1 = d$ and $x^{\ell+1} = T_{\Theta}^{\ell}(x^{\ell})$ for all $\ell \in [L]$.

Instead of an explicit cascade of distinct compositions, *implicit neural networks* \mathcal{N}_{Θ} use a single mapping T_{Θ} , and the output $\mathcal{N}_{\Theta}(d)$ is defined *implicitly* by an equation, e.g.

$$\mathcal{N}_{\Theta}(d) \triangleq x_d^* \text{ where } x_d^* = T_{\Theta}(x_d^*; d). \quad (6)$$

Equation (6) can be solved via a number of methods, e.g. fixed point iteration: $x^{k+1} = T_{\Theta}(x^k; d)$. Implicit neural networks recently received much attention as they admit a memory efficient backprop (Bai et al., 2019; 2020; Ghaoui et al., 2019; Fung et al., 2022). By construction, the output of $\mathcal{N}_{\Theta}(d)$ is a fixed point. Thus, several recent works explore using implicit networks in supervised learning problems where the target to be predicted can naturally be interpreted as a fixed point (Heaton et al., 2021; Gilton et al., 2021; Heaton, 2021).

3. Proposed Method: Nash-FPNs

We define a Nash fixed point network (N-FPN) \mathcal{N}_{Θ} as the solution to a parametrized variational inequality, i.e.

$$\mathcal{N}_{\Theta}(d) \triangleq \text{VI}(F_{\Theta}(\cdot; d), \mathcal{C}), \quad (7)$$

In our context, the set \mathcal{C} is a product of action sets \mathcal{V}_k and $F_{\Theta}(\cdot; \cdot)$ is a neural network with weights Θ . A similar approach was proposed in (Li et al., 2020); we discuss how our approach improves upon theirs in Section 4. First, we provide a novel theorem guaranteeing the proposed design has sufficient capacity to accurately approximate the correspondence $d \mapsto x_d^*$ for the games of interest.

Theorem 3.1. (UNIVERSAL APPROXIMATION) *If Assumptions (A1)–(A5) hold, then, for all $\varepsilon > 0$, there exists $F_{\Theta}(\cdot; \cdot)$ such that $\max_{d \in \mathcal{D}} \|x_d^* - \mathcal{N}_{\Theta}(d)\|_2 \leq \varepsilon$.*

Two core questions naturally arise for N-FPNs in (7):

- 1) For a given d , how are inferences of $\mathcal{N}_{\Theta}(d)$ computed?
- 2) How are weights Θ tuned using training data $\{d, x_d^*\}$?

We address each inquiry in turn. As is well-known (Facchinei & Pang, 2007), for all $\alpha > 0$,

$$\begin{aligned} x_d^{\circ} &\in \text{VI}(F_{\Theta}(\cdot; d), \mathcal{C}) \\ \iff x_d^{\circ} &= P_{\mathcal{C}}(x_d^{\circ} - \alpha F_{\Theta}(x_d^{\circ}; d)). \end{aligned} \quad (8)$$

where $P_{\mathcal{C}}$ denotes the projection onto \mathcal{C} , i.e. $P_{\mathcal{C}}(x) \triangleq \text{argmin}_{y \in \mathcal{C}} \|y - x\|^2$. When the operator $P_{\mathcal{C}} \circ (I - \alpha F_{\Theta})$ on the right hand side of (8) is tractable and well-behaved, inferences of $\mathcal{N}_{\Theta}(d)$ can be computed via a fixed point iteration, as in (Li et al., 2020). Unfortunately, for some \mathcal{C} computing $P_{\mathcal{C}}$ and $dP_{\mathcal{C}}/dz$ requires a number of operations scaling *cubicly* with the dimension of \mathcal{C} (Amos & Kolter, 2017), rendering this approach intractable for even moderately sized problems.

Our key insight is *there are multiple ways to turn (7) into a fixed point problem*. Thus, we propose a novel fixed point formulation which, while superficially more complicated, avoids expensive projections *and* is easy to backpropagate through. The key ingredient (see Theorem 3.2) is a novel use of three operator splitting (Davis & Yin, 2017), which admits simple and explicit formulae for each computation. To the best of our knowledge, this splitting has not appeared in the VI literature before. We present this architecture concretely as Algorithm 1. With a slight abuse of terminology, we refer to this architecture also as an N-FPN. Although we find Algorithm 1 to be most practical, we note other operator-based methods (e.g. ADMM and PDHG) can be used within the N-FPN framework via equivalences of different fixed point formulations of the VI.

Theorem 3.2. *Suppose $\mathcal{C} = \mathcal{C}_1 \cap \mathcal{C}_2$ for convex \mathcal{C}_1 and \mathcal{C}_2 . If both \mathcal{C}_i are polyhedral or have relative interiors with a point in common and the VI has a unique solution, then*

$$T_{\Theta}(x; d) \triangleq x - P_{\mathcal{C}_1}(x) + P_{\mathcal{C}_2}(2P_{\mathcal{C}_1}(x) - x - F_{\Theta}(P_{\mathcal{C}_1}(x); d)) \quad (9)$$

yields the equivalence

$$\mathcal{N}_{\Theta}(d) = x_d^{\circ} \iff x_d^{\circ} = P_{\mathcal{C}_1}(z_d^{\circ}) \text{ where } z_d^{\circ} = T_{\Theta}(z_d^{\circ}; d). \quad (10)$$

The fixed point operator T_Θ in (9) is computationally cheaper to evaluate than that in (8) when P_{C_1} and P_{C_2} are computationally cheaper than P_C . For example, suppose \mathcal{C} is a polytope written in general form: $\mathcal{C} = \{x : Ax = b \text{ and } x \geq 0\}$. Here, computing $P_C(x)$ amounts to solving the quadratic program $\min_{y \in \mathcal{C}} \|x - y\|_2^2$. However, we may instead take $\mathcal{C}_1 = \{x : Ax = b\}$ and $\mathcal{C}_2 = \{x : x \geq 0\}$, both of which enjoy straightforward closed-form projection operators P_{C_1} and P_{C_2} . Also, taking $\mathcal{C}_2 = \mathcal{C}$ and $\mathcal{C}_1 = \mathcal{X}$ (i.e. the whole space) reduces (10) to (8). For completeness, we present this special case of N-FPN as Algorithm 2, as this is more comparable to the approaches proposed in prior work (Ling et al., 2018; Li et al., 2020).

3.1. Forward propagation

Given the operator $T_\Theta(\cdot; d)$, there are many algorithms for determining its fixed point x_d° . Prior works (Ling et al., 2018; Li et al., 2020) use Newton-style methods, which are fast for small-scale and sufficiently smooth problems. But they may scale poorly to high dimensions (i.e. large $\dim(\mathcal{C})$). We employ Krasnosel’skiĭ-Mann (KM) iteration, which is the abstraction of splitting algorithms with low per-iteration computational and memory footprint. This is entirely analogous to the trade-off between first-order (e.g. gradient descent, proximal-gradient) and second-order methods (e.g. Newton) in high dimensional optimization; see (Ryu & Yin, 2022) for further discussion. The next theorem provides a sufficient condition under which KM iteration converges.

Theorem 3.3. *If \mathcal{C}^1 and \mathcal{C}^2 are as in Theorem 3.2 and if a sequence $\{z^k\}$ is generated via $z^{k+1} = T_\Theta(z^k, d)$ for T_Θ in (10) with F_Θ cocoercive, then $P_{C_1}(z^k) \rightarrow x_d^\circ = \mathcal{N}_\Theta(d)$.*

We simplify the iterate updates for T_Θ in (9) by introducing auxiliary sequences $\{x^k\}$ and $\{y^k\}$; see Algorithm 1.

Algorithm 2 N-FPN – Projected Gradient (Special Case)

1: $\mathcal{N}_\Theta(d)$:	◁ Input data is d
2: $x^1 \leftarrow \tilde{x}, n \leftarrow 2$,	◁ Initializations
3: $x^2 \leftarrow P_C(x^1 - F_\Theta(x^1; d))$	◁ Apply T update
4: while $\ x^n - x^{n-1}\ > \varepsilon$	◁ Loop to converge
5: $x^{n+1} \leftarrow P_C(x^n - F_\Theta(x^n; d))$	◁ Apply T update
6: $n \leftarrow n + 1$	◁ Iterate counter
7: return x^n	◁ Output inference

3.2. Further Constraint Decoupling

As discussed above, the architecture expressed in Algorithm 1 provides a massive computational speed-up over prior architectures when $\mathcal{C} = \mathcal{C}_1 \cap \mathcal{C}_2$ and P_{C_1} and P_{C_2} admit explicit and computationally cheap expressions, e.g.

when \mathcal{C} is a polytope. Yet, in many practical problems \mathcal{C} has a more complicated structure. For example, it may be the intersection of a large number of sets (i.e. $\mathcal{C} = \mathcal{C}_1 \cap \dots \cap \mathcal{C}_K$) or the Minkowski sum of intersections of simple sets (i.e. $\mathcal{C} = \mathcal{C}_1 + \dots + \mathcal{C}_K$ where $\mathcal{C}_k = \mathcal{C}_k^1 \cap \mathcal{C}_k^2$). We generalize our decoupling scheme by passing to a product space; see Propositions C.2 and C.4. With this extended decoupling we propose an N-FPN architecture with efficient forward propagation (i.e. evaluation of \mathcal{N}_Θ) and backward propagation (to tune weights Θ) using only the projection operators P_{C_k} (for the K -intersection case) or $P_{C_{k^i}}$ (for the Minkowski sum case); see Algorithms 3 and 4.

3.3. Backpropagation

Our second key contribution is to use the recently introduced Jacobian-Free Backprop (JFB) scheme (Fung et al., 2022) in training Nash-FPNs. For completeness, we describe how this applies to our proposed architecture. Consider a smooth loss function $\ell : \mathcal{X} \times \mathcal{X} \rightarrow \mathbb{R}$ and the training problem

$$\min_{\Theta} \mathbb{E}_{d \sim \mathcal{D}} [\ell(\mathcal{N}_\Theta(d), x_d^*)], \quad (11)$$

where we abusively interpret the data space \mathcal{D} as a distribution. Evaluation of an N-FPN consists of a fixed-point iteration, which may entail many iterations. To circumvent backpropagating through each forward step, the gradient $d\ell/d\Theta$ may be expressed by⁴

$$\frac{d\ell}{d\Theta} = \frac{d\ell}{dx} \frac{dx}{d\Theta} = \frac{d\ell}{dx} \frac{dP_{C^1}(z_d^\circ)}{dz} \frac{dz_d^\circ}{d\Theta}, \quad (12)$$

where the implicit function theorem (Krantz & Parks, 2012) is used to obtain the Jacobian-based equation

$$\frac{dz_d^\circ}{d\Theta} = \mathcal{J}_\Theta^{-1} \frac{\partial T_\Theta}{\partial \Theta}, \quad \text{with } \mathcal{J}_\Theta \triangleq \text{Id} - \frac{dT_\Theta}{dz}. \quad (13)$$

For large-scale games, solving (13) is computationally intensive. Instead, we employ JFB, which consists of replacing \mathcal{J}_Θ^{-1} in (13) with the identity matrix. This substitution yields a preconditioned gradient and is effective for training in image classification (Fung et al., 2022) and data-driven CT reconstructions (Heaton et al., 2021). Importantly, using JFB only requires backpropagating through a *single* application of T_Θ (i.e. the final forward step).

3.4. Limitations

Our approach tunes an operator so its fixed points match given contextual Nash equilibria, but says little about the players’ cost functions. Thus, T_Θ cannot be used to design interventions to increase social welfare (i.e. the negative of the sum of all players costs) (Ratliff et al., 2014; Konstantakopoulos et al., 2014; Li et al., 2020). However, T_Θ can be used to design interventions to discourage agents from playing a given action.

⁴All arguments are implicit and use N-FPNs defined by (10).

Algorithm 1 Nash Fixed Point Network (Abstract Form)

<pre> 1: $\mathcal{N}_\Theta(d)$: 2: $z^1 \leftarrow \tilde{z}, z^0 \leftarrow \tilde{z}, n \leftarrow 1$ 3: while $\ z^n - z^{n-1}\ > \varepsilon$ or $n = 1$ 4: $x^{n+1} \leftarrow P_{\mathcal{C}^1}(z^n)$ 5: $y^{n+1} \leftarrow P_{\mathcal{C}^2}(2x^{n+1} - z^n - F_\Theta(x^{n+1}; d))$ 6: $z^{n+1} \leftarrow z^n - x^{n+1} + y^{n+1}$ 7: $n \leftarrow n + 1$ 8: return $P_{\mathcal{C}^1}(z^n)$ </pre>	<pre> \triangleleft Input data is d \triangleleft Initialize iterates and counter \triangleleft Loop to convergence at fixed point \triangleleft Project onto constraint set \triangleleft Project reflected gradient \triangleleft Combine auxiliary sequences \triangleleft Increment counter \triangleleft Output inference </pre>
---	--

4. Related Works

There are two distinct learning problems for games. The first considers repeated rounds of the same game and operates from the player’s perspective. The players are assumed to have imperfect knowledge of the game, and the goal is to learn the optimal strategy (*i.e.* the Nash equilibrium or, more generally, a coarse correlated equilibrium), given only the cost incurred in each round. This problem is not investigated in this work, and we refer the reader to (Hannan, 1957; Stoltz & Lugosi, 2007; Sessa et al., 2020) for further details.

The second problem supposes historical observations of agents’ behaviour are available to an external observer. For example, (Waugh et al., 2011; Ratliff et al., 2014; Konstantakopoulos et al., 2014; Bertsimas et al., 2015; Zhang et al., 2016; Zhang & Paschalidis, 2017; Zhang et al., 2018; Allen et al., 2021) assume access to (noisy) observations of the Nash equilibrium of a *non-contextual* game, propose a parametrized form of each players cost function, and then select these parameters by solving a regression problem. We emphasize that this approach does not allow for cost functions depending on the context d .

Several recent works (Ling et al., 2018; 2019; Li et al., 2020) consider data consisting of pairs of contexts d and equilibria x_d^* of the contextual game parameterized by d , and employ techniques from contemporary deep learning. Crucially, (Ling et al., 2018) is the first paper to propose a differentiable game solver for two player games, allowing for end-to-end training of a neural network that predicts x_d^* given d . In (Ling et al., 2019), this approach was modified, leading to a faster backpropagation algorithm, but only for two-player games admitting a compact extensive form representation. Both (Ling et al., 2018; 2019) only consider two player games where \mathcal{C} is the product of two simplices *and* assumes the game is regularized in such a way that x_d^* is guaranteed to lie in the interior of \mathcal{C} , thus sidestepping the tricky issue of projection to \mathcal{C} .

In (Li et al., 2020) a differentiable variational inequality layer (VI-Layer), similar to (7), is proposed. Using the equivalence (8), they convert the problem of training this

VI-Layer to that of tuning a parametrized operator $F_\Theta(x_d^*; d)$ such that

$$x_d^* \approx P_{\mathcal{C}}(x_d^* - F_\Theta(x_d^*; d)).$$

This idea is a significant step forward as it extends the approach of (Ling et al., 2018) to unregularized games with arbitrary \mathcal{C} and arbitrary number of players. However, as (Ling et al., 2018) does not use constraint decoupling (see Theorem 3.2 and Section 3.2) they are forced to use an iterative $\mathcal{O}(\dim(\mathcal{C})^3)$ algorithm (Amos & Kolter, 2017) to compute $P_{\mathcal{C}}$ (resp. $dP_{\mathcal{C}}/dz$) in every forward (resp. backward) pass. When $F_\Theta(x_d^*; d)$ is a multi-layer neural network, tuning Θ might require millions of forward and backward passes. Thus, their approach is impractical for games with even moderately large \mathcal{C} (see Section 3.3 of (Amos & Kolter, 2017)).

Finally, we note (Ling et al., 2018; 2019; Li et al., 2020) use the costly Jacobian-based backpropagation (see Section 3.3) when training. Moreover, the network architectures proposed in these works are not compatible with Jacobian-free backpropagation, whereas N-FPN is. The use of JFB makes training N-FPNs significantly faster, as shown in Section 5.1.

5. Numerical Examples

We show the efficacy of N-FPNs on two classes of contextual games: symmetric matrix games and traffic routing.

5.1. Contextual Matrix Games

In (Ling et al., 2018) the Payoff-Net architecture is used for a contextual “rock-paper-scissors” game. This is a (symmetric) matrix game where both players have action sets of dimension 3. Note they consider *entropy-regularized* cost functions⁵:

$$u_1(x; d) = x_2^\top B(d)x_1 + \sum_i x_{1,i} \log(x_{1,i})$$

$$u_2(x; d) = -x_2^\top B(d)x_1 + \sum_i x_{2,i} \log(x_{2,i}),$$

⁵equivalently: they determine the Quantal Response Equilibrium not the Nash Equilibrium

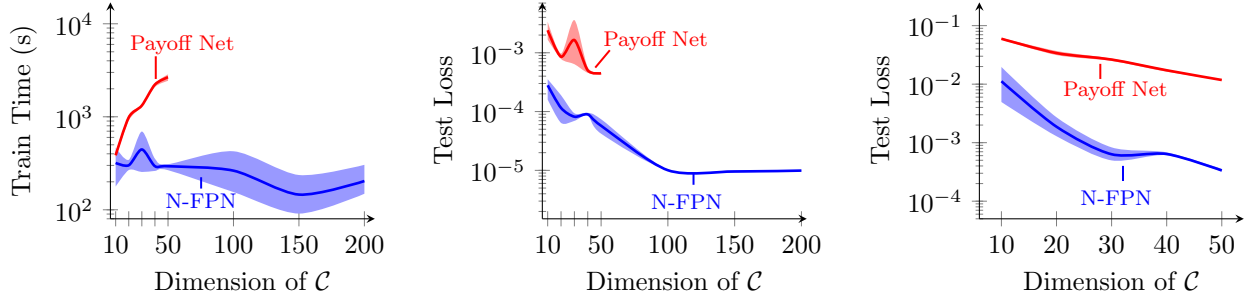


Figure 2. Total training time (left) and final test loss (center) for Nash-FPN and Payoff-Net for matrix games of increasing size a , trained for 100 epochs or until a test loss less than 10^{-5} is achieved. The final test loss decreases as a function of a , which is expected since the number of parameters increases with a . The right plot shows the results of training for ten epochs only, showing training N-FPN rapidly finds parameters achieving a low test loss.

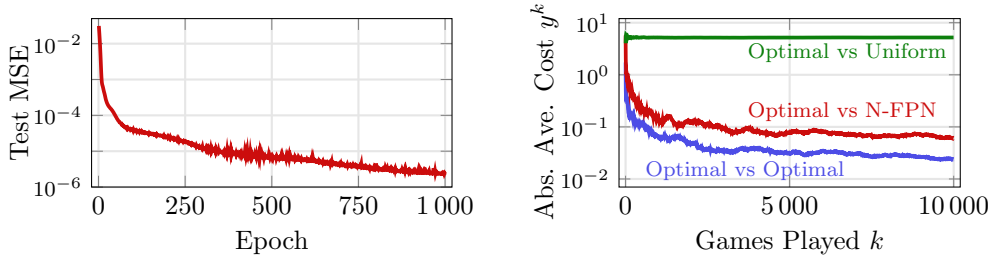


Figure 3. Rock-paper-scissors example. Left plot shows N-FPN test loss during training. Right plot shows the cost expression y^k over the course of k games in three settings. The first player always acts optimally, knowing both the true cost $u_1(\cdot; d)$ and the second player’s strategy. The second player either also acts optimally, chooses uniformly randomly, or uses N-FPN predictions only knowing d . Both players acting optimally yields a Nash equilibrium, making $y^k \rightarrow 0$. When the second player is uniform, the first player typically wins. This plot shows the N-FPN player chooses nearly optimally.

for antisymmetric contextual cost matrix $B(d) \in \mathbb{R}^{a \times a}$, thus guaranteeing the game satisfies assumptions (A1)–(A5), particularly (A4). We do the same here. Each player’s set of mixed strategies is the probability simplex $\Delta^a \triangleq \{x \in \mathbb{R}_{\geq 0}^a : \|x\|_1 = 1\} \subset \mathbb{R}^a$ so $\mathcal{C} = \Delta^a \times \Delta^a$. We vary a in multiples of 5 from 5 to 25. For each a we generate a training data set $\{(d^i, x_{d^i}^*)\}_{i=1}^{2000}$ and train a Payoff-Net and an N-FPN with comparable numbers of parameters—see Appendix D.1 for details—for 100 epochs or until the test loss is below 10^{-5} , whichever comes first. For N-FPN only we also consider data sets where $a = 50, 75$ and 100. The results are presented in Figure 2. As is clear, N-FPN trains several orders of magnitude faster (and to a higher accuracy) than Payoff-Net. We attribute this to the advantage Jacobian-Free Backprop (JFB) enjoys over the conventional Jacobian-based backprop employed by Payoff-Net⁶. We note that the N-FPN architecture easily extends to games with more than two players and to un-regularized matrix games, whereas it is unclear how Payoff-Net might be adapted to these situations.

⁶We note that Payoff-Net cannot simply be trained using JFB, as the computation of Jacobians is central to its forward pass too

For illustration, we simulate play between two players for $a = 3$ (*i.e.* the “rock-paper-scissors” case). The first player acts optimally using knowledge of $B(d)$ and the second player’s strategy. Three options are used for the second player: another optimal player, an N-FPN player that only has access to d , and uniform choices. With two optimal players, a Nash equilibria is obtained where the expected cost after each game is zero. If the N-FPN is well-trained, then the second case yields the same result. In the final case, the optimal player has an advantage, yielding first player costs less than zero (*i.e.* the first player usually wins). Here

(Expected Abs. Nash Player k -Game Average Cost) $\equiv y^k$

$$\triangleq \mathbb{E}_{d \sim \mathcal{D}} \left[\left| \frac{1}{k} \sum_{\ell=1}^k u_1(s^\ell; d) \right| \right], \quad (14)$$

where s^k is a tuple of two one-hot vectors (*e.g.* $s_1^k \sim x_d^*$ and $s_2^k \sim \mathcal{N}_\Theta(d)$). If $\mathcal{N}_\Theta(d) = x_d^*$, then the expected cost u_1 is zero and $y^k \rightarrow 0$ (*n.b.* simulated games have nonzero variance due to one-hot sampling s_i^k whereas x_d^* is continuous). This behavior is illustrated in Figure 3.

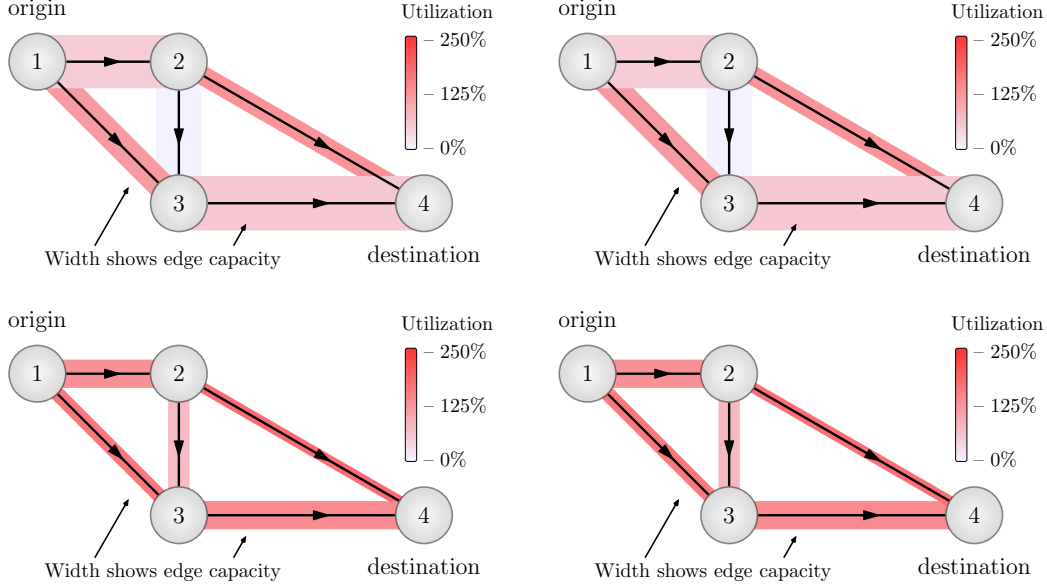


Figure 4. Top left: True traffic flow for “sunny” context. Top right: Predicted traffic by \mathcal{N}_Θ for “sunny” context. Bottom left: True traffic flow for “rainy” context. Bottom right: Predicted traffic by \mathcal{N}_Θ for “rainy” context

5.2. Contextual Traffic Routing

Setup Consider a road network represented by a directed graph with vertices V and arcs E . Let $N \in \mathbb{R}^{|V| \times |E|}$ denote the vertex-arc incidence matrix (see Appendix D.2). An origin-destination pair (OD-pair) is a triple (v_1, v_2, q) with $v_i \in V$ and $q \in \mathbb{R}_{>0}$, encoding the constraint of routing q units of traffic from v_1 to v_2 . Each OD-pair is encoded by a vector $b \in \mathbb{R}^{|V|}$ with $b_{v_1} = -q$, $b_{v_2} = q$ and all other entries zero. A valid *traffic flow* $x \in \mathbb{R}^{|E|}$ for an OD-pair has nonnegative entries satisfying the flow equation $Nx = b$. The e -th entry x_e represents the traffic density along the e -th arc. The flow equation ensures the number of cars entering an intersection equals the number leaving, except a net movement of q units of traffic from v_1 to v_2 . For K OD-pairs, a valid traffic flow x is the sum of traffic flows for each OD-pair, which is in the Minkowski sum:

$$\mathcal{C} = \sum_{k=1}^K \mathcal{C}_k \triangleq \underbrace{\{x : Nx = b_k\}}_{\mathcal{C}_k^1} \cap \underbrace{\{x : x \geq 0\}}_{\mathcal{C}_k^2}, \quad (15)$$

A *contextual travel time function* $t_e(x_e; d)$ is associated with each arc, where d encodes contextual data. This function increases monotonically with x_e , reflecting the fact that increased congestion leads to longer travel times. The context d encodes exogenous factors — weather, construction and so on. Here the equilibrium of interest is, roughly speaking, a flow configuration x_d^* where the travel time between each OD-pair is as short as possible when taking into account

congestion effects (Carlier & Santambrogio, 2012). This is known as a *Wardrop equilibrium* (also called the *user equilibrium*) (Wardrop, 1952), a special case of Nash equilibria where

$F = [t_1(x_1; d)^\top \cdots t_{|E|}(x_{|E|}; d)^\top]^\top$. In certain cases, a Wardrop equilibrium is the limit of a sequence of Nash equilibria as the number of drivers goes to infinity (Paccagnan et al., 2018).

TRAFIX Scores Accuracy of traffic routing predictions are measured by a *TRAFIX score*. This score forms an intuitive alternative to mean squared error. An error tolerance $\varepsilon > 0$ is chosen (*n.b.* $\varepsilon = 5 \times 10^{-3}$ in our experiments). For an estimate x of x^* , the TRAFIX score with parameter ε is the percentage of edges for which x has relative error (with tolerance⁷ $\tau > 0$) less than ε , *i.e.*

$$(\text{rel. error of edge } e) \triangleq \frac{|x_e - x_e^*|}{|x_e^*| + \tau}, \quad (16a)$$

$$\text{TRAFIX}(x, x^*; \varepsilon, \tau) \triangleq \frac{(\# \text{ edges with rel. error} < \varepsilon)}{(\# \text{ edges})} \times 100\%. \quad (16b)$$

Our plots and tables show the expected TRAFIX scores over the distributions of testing data.

Datasets and Training We are unaware of any prior datasets for contextual traffic routing, and so we construct

⁷The parameter τ is added to handle the case when the e -th component of x^* is zero, *i.e.* $x_e^* = 0$.

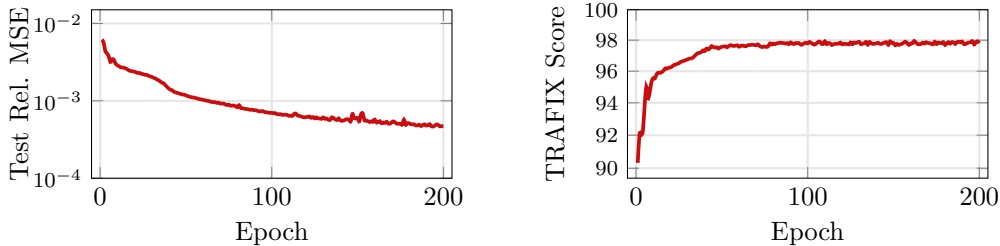


Figure 5. Plots for N-FPN performance on Eastern Massachusetts testing data. The left plot shows convergence of expected relative mean squared error on testing data after each training epoch and the right shows the expected TRAFIX score on testing data after each training epoch.

dataset	edges/nodes	OD-pairs	# params	rel. MSE	TRAFIX score
Sioux Falls	76/24	528	46K	1.9×10^{-3}	94.42%
Eastern Massachusetts	258/74	1113	99K	4.7×10^{-4}	97.94%
Berlin-Friedrichshain	523/224	506	179K	5.3×10^{-4}	97.42%
Berlin-Tiergarten	766/361	644	253K	7.6×10^{-4}	95.95%
Anaheim	914/416	1406	307K	2.4×10^{-3}	95.28%

Table 2. Expected values of N-FPN predictions on traffic routing test data. First and second columns show the number of edges, nodes, and origin-destination pairs for corresponding dataset. Second column shows number of tunable parameters. Further details may be found in Appendix D.5.

our own. First, we construct a toy example based on the “Braess paradox” network studied in (Li et al., 2020), illustrated in Figure 4. Here $d \in \mathbb{R}^5$; see Appendix D for further details.

We also constructed contextual traffic routing data sets based on road networks of real-world cities curated by the Transportation Networks for Research Project (tra). We did so by fixing a choice of $t_e(x; d)$ for each arc e , randomly generating a large set of contexts $d \in [0, 1]^{10}$ and then, for each d , finding a solution $x_d^* \in \text{VI}(F(\cdot; d), \mathcal{C})$. Table 2 shows a description of the traffic networks datasets, including the numbers of edges, nodes, and OD-pairs. Further details are in Appendix D. We emphasize that for these contextual games the structure of \mathcal{C} is complex; it is a Minkowski sum of hundreds of high-dimensional polytopes (recall Equation (15)). We train an N-FPN using the constraint decoupling described in Section 3.2 for forward propagation (see Algorithm 3) to predict x_d^* from d for each data set with architectures as described in Appendix D.5. Additional training details are in Appendix D.6.

Results As illustrated in Figure 4, the N-FPN almost perfectly predicts the resulting Wardrop equilibrium given only the context d . The results for the real-world networks are shown in the final two columns of Table 2. The convergence during training of the relative MSE and TRAFIX score on the Eastern-Massachusetts testing dataset is shown in Figure 5. Additional plots can be found in Appendix F.

6. Conclusions

The fusion of big data and optimization algorithms offers potential for predicting equilibria in systems with many interacting agents. The proposed N-FPNs form a *scalable* data-driven framework for efficiently predicting equilibria for such systems that can be modeled as contextual games. The N-FPN architecture yields equilibria outputs that satisfy constraints while also being trained end-to-end. Moreover, the provided constraint decoupling schemes enable simple forward and backward propagation using explicit formulae for each projection. The efficacy of N-FPNs is illustrated on large-scale traffic routing problems using a contextual traffic routing benchmark dataset and TRAFIX scoring system. Future work will investigate applications on larger datasets, convergence acceleration, and incorporation of distributed algorithms for training.

References

- Transportation Networks for Research Core Team. Transportation Networks for Research. <https://github.com/bstabler/TransportationNetworks>. Accessed: 2021-05-24.
- Allen, S., Dickerson, J. P., and Gabriel, S. A. Using inverse optimization to learn cost functions in generalized Nash games. *arXiv preprint arXiv:2102.12415*, 2021.
- Amos, B. and Kolter, J. Z. Optnet: Differentiable optimization as a layer in neural networks. In *International*

- Conference on Machine Learning*, pp. 136–145. PMLR, 2017.
- Arrow, K. J. and Debreu, G. Existence of an equilibrium for a competitive economy. *Econometrica: Journal of the Econometric Society*, pp. 265–290, 1954.
- Azar, O. H. and Bar-Eli, M. Do soccer players play the mixed-strategy nash equilibrium? *Applied Economics*, 43(25):3591–3601, 2011.
- Bai, S., Kolter, J. Z., and Koltun, V. Deep equilibrium models. In *Advances in Neural Information Processing Systems*, pp. 690–701, 2019.
- Bai, S., Koltun, V., and Kolter, J. Z. Multiscale deep equilibrium models. *Advances in Neural Information Processing Systems*, 33, 2020.
- Bauschke, H. H., Combettes, P. L., et al. *Convex Analysis and Monotone Operator Theory in Hilbert Spaces*. Springer, 2nd edition, 2017.
- Bertsimas, D., Gupta, V., and Paschalidis, I. C. Data-driven estimation in equilibrium using inverse optimization. *Mathematical Programming*, 153(2):595–633, 2015.
- Bisong, E. Google colab. In *Building Machine Learning and Deep Learning Models on Google Cloud Platform*, pp. 59–64. Springer, 2019.
- Carlier, G. and Santambrogio, F. A continuous theory of traffic congestion and Wardrop equilibria. *Journal of Mathematical Sciences*, 181(6):792–804, 2012.
- Cegielski, A. *Iterative methods for fixed point problems in Hilbert spaces*, volume 2057. Springer, Berlin, Germany, 2012.
- Chen, T., Chen, X., Chen, W., Heaton, H., Liu, J., Wang, Z., and Yin, W. Learning to optimize: A primer and a benchmark. *arXiv preprint arXiv:2103.12828*, 2021.
- Dafermos, S. Sensitivity analysis in variational inequalities. *Mathematics of Operations Research*, 13(3):421–434, 1988.
- Davis, D. and Yin, W. A three-operator splitting scheme and its optimization applications. *Set-valued and variational analysis*, 25(4):829–858, 2017.
- de Avila Belbute-Peres, F., Smith, K., Allen, K., Tenenbaum, J., and Kolter, J. Z. End-to-end differentiable physics for learning and control. *Advances in neural information processing systems*, 31:7178–7189, 2018.
- Facchinei, F. and Pang, J.-S. *Finite-dimensional variational inequalities and complementarity problems*. Springer Science & Business Media, 2007.
- Fung, S. W., Heaton, H., Li, Q., McKenzie, D., Osher, S., and Yin, W. Jfb: Jacobian-free Backpropagation for Implicit Networks. *Proceedings of the AAAI Conference on Artificial Intelligence*, 2022.
- Ghaoui, L. E., Gu, F., Travacca, B., Askari, A., and Tsai, A. Y. Implicit deep learning. *arXiv preprint arXiv:1908.06315*, 2019.
- Gilton, D., Ongie, G., and Willett, R. Deep equilibrium architectures for inverse problems in imaging. *arXiv preprint arXiv:2102.07944*, 2021.
- Hannan, J. Approximation to Bayes risk in repeated play. *Contributions to the Theory of Games*, 21(39):97, 1957.
- Heaton, H., Fung, S. W., Gibali, A., and Yin, W. Feasibility-based fixed point networks. *arXiv preprint arXiv:2104.14090*, 2021.
- Heaton, H. W. *Learning to Optimize with Guarantees*. PhD thesis, University of California, Los Angeles, 2021.
- Jahn, O., Möhring, R. H., Schulz, A. S., and Stier-Moses, N. E. System-optimal routing of traffic flows with user constraints in networks with congestion. *Operations research*, 53(4):600–616, 2005.
- Kidger, P. and Lyons, T. Universal approximation with deep narrow networks. In *Conference on learning theory*, pp. 2306–2327. PMLR, 2020.
- Kingma, D. P. and Ba, J. Adam: A method for stochastic optimization. In *ICLR (Poster)*, 2015.
- Konstantakopoulos, I. C., Ratliff, L. J., Jin, M., Sastry, S. S., and Spanos, C. Social game for building energy efficiency: Utility learning, simulation, and analysis. *arXiv preprint arXiv:1407.0727*, 2014.
- Kotary, J., Fioretto, F., Van Hentenryck, P., and Wilder, B. End-to-end constrained optimization learning: A survey. *arXiv preprint arXiv:2103.16378*, 2021.
- Krantz, S. G. and Parks, H. R. *The implicit function theorem: history, theory, and applications*. Springer Science & Business Media, 2012.
- Krasnosel’skii, M. Two remarks about the method of successive approximations. *Uspekhi Mat. Nauk*, 10:123–127, 1955.
- LeBlanc, L. J., Morlok, E. K., and Pierskalla, W. P. An efficient approach to solving the road network equilibrium traffic assignment problem. *Transportation research*, 9(5):309–318, 1975.
- Li, J., Yu, J., Nie, Y., and Wang, Z. End-to-end learning and intervention in games. *Advances in Neural Information Processing Systems*, 33, 2020.

- Ling, C. K., Fang, F., and Kolter, J. Z. What game are we playing? end-to-end learning in normal and extensive form games. *arXiv preprint arXiv:1805.02777*, 2018.
- Ling, C. K., Fang, F., and Kolter, J. Z. Large scale learning of agent rationality in two-player zero-sum games. In *Proceedings of the AAAI Conference on Artificial Intelligence*, volume 33, pp. 6104–6111, 2019.
- Mann, R. Mean Value Methods in Iteration. 4(3):506–510, 1953.
- Nash, J. F. Equilibrium points in n-person games. *Proceedings of the national academy of sciences*, 36(1):48–49, 1950.
- Paccagnan, D., Gentile, B., Parise, F., Kamgarpour, M., and Lygeros, J. Nash and Wardrop equilibria in aggregative games with coupling constraints. *IEEE Transactions on Automatic Control*, 64(4):1373–1388, 2018.
- Ratliff, L. J., Jin, M., Konstantakopoulos, I. C., Spanos, C., and Sastry, S. S. Social game for building energy efficiency: Incentive design. In *2014 52nd Annual Allerton Conference on Communication, Control, and Computing (Allerton)*, pp. 1011–1018. IEEE, 2014.
- Rockafellar, R. T. *Convex analysis*, volume 36. Princeton university press, 1970.
- Rosen, J. B. Existence and uniqueness of equilibrium points for concave n-person games. *Econometrica: Journal of the Econometric Society*, pp. 520–534, 1965.
- Roughgarden, T. Routing games. *Algorithmic game theory*, 18:459–484, 2007.
- Ryu, E. and Yin, W. *Large-Scale Convex Optimization: Algorithm Designs via Monotone Operators*. Cambridge University Press, Cambridge, England, 2022.
- Sessa, P. G., Bogunovic, I., Krause, A., and Kamgarpour, M. Contextual games: Multi-agent learning with side information. *Advances in Neural Information Processing Systems*, 33, 2020.
- Stoltz, G. and Lugosi, G. Learning correlated equilibria in games with compact sets of strategies. *Games and Economic Behavior*, 59(1):187–208, 2007.
- Wardrop, J. G. Some theoretical aspects of road traffic research. *Proceedings of the institution of civil engineers*, 1(3):325–362, 1952.
- Waugh, K., Ziebart, B. D., and Bagnell, J. A. Computational rationalization: the inverse equilibrium problem. In *Proceedings of the 28th International Conference on International Conference on Machine Learning*, pp. 1169–1176, 2011.
- Winston, E. and Kolter, J. Z. Monotone operator equilibrium networks. In Larochelle, H., Ranzato, M., Hadsell, R., Balcan, M. F., and Lin, H. (eds.), *Advances in Neural Information Processing Systems*, volume 33, pp. 10718–10728. Curran Associates, Inc., 2020. URL <https://proceedings.neurips.cc/paper/2020/file/798d1c2813cbdf8bcdb388db0e32d496-Paper.pdf>.
- Zhang, J. and Paschalidis, I. C. Data-driven estimation of travel latency cost functions via inverse optimization in multi-class transportation networks. In *2017 IEEE 56th Annual Conference on Decision and Control (CDC)*, pp. 6295–6300. IEEE, 2017.
- Zhang, J., Pourazarm, S., Cassandras, C. G., and Paschalidis, I. C. The price of anarchy in transportation networks by estimating user cost functions from actual traffic data. In *2016 IEEE 55th Conference on Decision and Control (CDC)*, pp. 789–794. IEEE, 2016.
- Zhang, J., Pourazarm, S., Cassandras, C. G., and Paschalidis, I. C. The price of anarchy in transportation networks: Data-driven evaluation and reduction strategies. *Proceedings of the IEEE*, 106(4):538–553, 2018.

A. Proofs of theorems

Here we provide proofs for all theorems stated in the main text. For the readers convenience we reproduce each statement before proving it.

Theorem 2.1. Suppose the following assumptions hold:

- (A1) $\mathcal{C} \subset \mathcal{X}$ is closed and convex.
- (A2) The cost functions $u_k(x; d)$ are continuously differentiable with respect to x .
- (A3) For all x , each $\nabla_k u_k(x; \cdot)$ is Lipschitz.
- (A4) Each cost function $u_k(x_k, x_{-k}; d)$ is α -strongly convex with respect to x_k .
- (A5) The set of contextual data \mathcal{D} is compact.

Then:

- (1) There is a unique Nash Equilibrium x_d° for all $d \in \mathcal{D}$.
- (2) The map $d \mapsto x_d^\circ$ is Lipschitz continuous.

Proof. (A3) implies the game gradient $F(\cdot; d)$ is strictly (in fact, strongly) monotone for all d :

$$\langle F(x; d) - F(y; d), x - y \rangle > 0 \quad \forall x, y \quad (17)$$

In game theory this is sometimes referred to as *diagonal strict convexity*. By (Rosen, 1965, Theorem 2) the Nash equilibrium x_d^* is unique. See also (Facchinei & Pang, 2007, Theorem 2.2.3). This proves part 1.

For part 2, first observe that (A4) implies F is Lipschitz continuous with respect to d while (A5) guarantees F is α strongly monotone. (Dafermos, 1988, Theorem 2.1) then shows that around any fixed $\bar{d} \in \mathcal{D}$ the map $d \mapsto x_d^*$ is locally Lipschitz, *i.e.* there exists a constant $L_{\bar{d}}$ and an open neighborhood $N_{\bar{d}} \subset \mathcal{D}$ of \bar{d} upon which $d \mapsto x_d^*$ is $L_{\bar{d}}$ -Lipschitz continuous. As $\bar{\mathcal{D}}$ is compact a standard covering argument converts this local Lipschitz property to a global Lipschitz property. \square

Theorem 3.1. If Assumptions (A1) to (A5) hold, then for any $\varepsilon > 0$ there exists an $F_{\Theta}(\cdot; \cdot)$ such that

$$\max_{d \in \mathcal{D}} \|x_d^* - \mathcal{N}_{\Theta}(d)\|_2 \leq \varepsilon. \quad (18)$$

Proof. Let $\varepsilon > 0$ be given. Denote the map $d \mapsto x_d^*$ by \mathcal{L} , *i.e.* $\mathcal{L}(d) \triangleq x_d^*$. By Theorem 2.1, \mathcal{L} is well-defined and Lipschitz continuous. Combined with the compactness of \mathcal{D} via (A5), this implies, by standard universal approximation properties of neural networks (Kidger & Lyons, 2020), there exists a continuous neural network $G_{\Theta} : \mathcal{D} \rightarrow \mathcal{X}$ such that

$$\max_{d \in \mathcal{D}} \|\mathcal{L}(d) - G_{\Theta}(d)\|_2 \leq \frac{\varepsilon}{2}. \quad (19)$$

Next fix $\alpha > 0$ and define the operator $F_{\Theta} : \mathcal{X} \times \mathcal{D} \rightarrow \mathcal{X}$ by

$$F_{\Theta}(x; d) \triangleq \frac{x - G_{\Theta}(d)}{\alpha}. \quad (20)$$

and recall the corresponding N-FPN is defined as

$$\mathcal{N}_{\Theta}(d) \triangleq \text{VI}(F_{\Theta}(\cdot; d), \mathcal{C}). \quad (21)$$

Note F_{Θ} is continuous by the continuity of G_{Θ} , and so the VI and fixed point equivalence (8) implies, for any $\zeta \in \mathcal{D}$,

$$\mathcal{N}_{\Theta}(\zeta) = P_{\mathcal{C}}(x_{\zeta}^{\circ} - \alpha F_{\Theta}(x_{\zeta}^{\circ}; d)) = P_{\mathcal{C}}(G_{\Theta}(\zeta)). \quad (22)$$

By definition of the projection $P_{\mathcal{C}}$,

$$\|P_{\mathcal{C}}(G_{\Theta}(\zeta)) - G_{\Theta}(\zeta)\|_2 = \min_{x \in \mathcal{C}} \|x - G_{\Theta}(\zeta)\|_2, \quad (23)$$

which implies, since $\mathcal{L}(\zeta) \in \mathcal{C}$,

$$\|P_{\mathcal{C}}(G_{\Theta}(\zeta)) - G_{\Theta}(\zeta)\|_2 \leq \|\mathcal{L}(\zeta) - G_{\Theta}(\zeta)\|_2. \quad (24)$$

Together with the triangle inequality, (19) and (24) yield

$$\|x_{\zeta}^* - \mathcal{N}_{\Theta}(\zeta)\|_2 = \|\mathcal{L}(\zeta) - P_{\mathcal{C}}(G_{\Theta}(\zeta))\|_2 \quad (25a)$$

$$\leq \|\mathcal{L}(\zeta) - G_{\Theta}(\zeta)\|_2 + \|G_{\Theta}(\zeta) - P_{\mathcal{C}}(G_{\Theta}(\zeta))\|_2 \quad (25b)$$

$$\leq 2\|\mathcal{L}(\zeta) - G_{\Theta}(\zeta)\|_2 \quad (25c)$$

$$= \varepsilon. \quad (25d)$$

Since (25) holds for arbitrarily chosen $\zeta \in \mathcal{D}$, we deduce (18) holds for the provided ε . As $\varepsilon > 0$ was also arbitrarily chosen, the result follows. \square

B. Variational Inequalities

Below we provide a lemma justifying the decoupling of constraints in the action set \mathcal{C} . Here we make use of polyhedral sets⁸; however, this result also holds in a more general setting utilizing relative interiors of \mathcal{C}^1 and \mathcal{C}^2 . By $\delta_{\mathcal{C}} : \mathcal{X} \rightarrow \mathbb{R} \cup \{+\infty\}$ we denote the indicator function defined such that $\delta_{\mathcal{C}}(x) = 0$ in \mathcal{C} and $+\infty$ elsewhere. The subgradient of the indicator function (also known as the normal cone of \mathcal{C}) is denoted by $\partial\delta_{\mathcal{C}}$.

Lemma B.1. For⁹ operator $F : \mathcal{X} \rightarrow \mathcal{X}$ and polyhedral sets $\mathcal{C}^1, \mathcal{C}^2 \subset \mathcal{X}$ such that $\mathcal{C} = \mathcal{C}^1 \cap \mathcal{C}^2$

$$x_d^{\circ} \in \text{VI}(F(\cdot; d), \mathcal{C}) \quad (26a)$$

$$\iff 0 \in F(x_d^{\circ}; d) + \partial\delta_{\mathcal{C}^1}(x_d^{\circ}) + \partial\delta_{\mathcal{C}^2}(x_d^{\circ}) \quad (26b)$$

$$\iff x_d^{\circ} = P_{\mathcal{C}^1}(z^{\circ}), \text{ where } z^{\circ} = T(z^{\circ}; d). \quad (26c)$$

Proof. We begin with the well-known equivalence relation (Facchinei & Pang, 2007)

$$x_d^{\circ} \in \text{VI}(F(\cdot; d), \mathcal{C}) \iff 0 \in F(x_d^{\circ}; d) + \partial\delta_{\mathcal{C}}(x_d^{\circ}). \quad (27)$$

Because \mathcal{C}^1 and \mathcal{C}^2 are polyhedral sets, we may apply (Rockafellar, 1970, Theorem 23.8.1) to assert

$$\partial\delta_{\mathcal{C}} = \partial\delta_{\mathcal{C}^1} + \partial\delta_{\mathcal{C}^2}. \quad (28)$$

Next consider three maximal¹⁰ monotone operators A , B and C , with C single-valued. For each $\alpha > 0$, let $J_{\alpha A}$ and $R_{\alpha A}$ be the resolvent of αA and reflected resolvent of αA , respectively, *i.e.*

$$J_{\alpha A} \triangleq (I + \alpha A)^{-1} \quad \text{and} \quad R_{\alpha A} \triangleq 2J_{\alpha A} - I. \quad (29)$$

In particular, note the resolvent of $\partial\delta_{\mathcal{C}^i}$ is precisely the projection operator $P_{\mathcal{C}^i}$ (Bauschke et al., 2017, Example 23.4). Using three operator splitting (*e.g.* see (Davis & Yin, 2017, Lemma 2.2) and (Ryu & Yin, 2022)), we obtain the equivalence

$$0 \in (A + B + C)(x) \iff x = J_{\alpha B}(z), \text{ where } z = z - J_{\alpha B}(z) + J_{\alpha A}(R_{\alpha B} - \alpha C J_{\alpha B})(z). \quad (30)$$

⁸A set is polyhedral if it is of the form $\{x : \langle x, a^i \rangle \leq b_i, \text{ for } i \in [p]\}$, for $p \in \mathbb{N}$.

⁹Here and in Appendix C we suppress the dependence of F on d for brevity.

¹⁰A monotone operator M is *maximal* if there is no other monotone operator S such that $\text{Gra}(M) \subset \text{Gra}(S)$ properly (Ryu & Yin, 2022). This is a technical assumption that holds for all cases of our interest.

Setting $A = \partial\delta_{\mathcal{C}^2}$, $B = \partial\delta_{\mathcal{C}^1}$, and $C = F$, (30) reduces to

$$\begin{aligned} 0 &\in F(x_d^\circ; d) + \partial\delta_{\mathcal{C}^1}(x_d^\circ) + \partial\delta_{\mathcal{C}^2}(x_d^\circ) \\ \iff x_d^\circ &= P_{\mathcal{C}^1}(z_d^\circ), \text{ where } z_d^\circ = T(z_d^\circ; d). \end{aligned} \quad (31)$$

Combining (27), (28), and (31) yields (26), as desired. \square

We next restate and provide a brief proof for the main convergence theorem.

Theorem 3.3. If \mathcal{C}^1 and \mathcal{C}^2 are as in Theorem 3.2 and if a sequence $\{z^k\}$ is generated via $z^{k+1} = T_\Theta(z^k, d)$ for T_Θ in (10) with F_Θ cocoercive, then $P_{\mathcal{C}^1}(z^k) \rightarrow x_d^\circ = \mathcal{N}_\Theta(d)$.

Proof. Because all sets considered in this work are closed and convex, the projection operators $P_{\mathcal{C}^1}$ and $P_{\mathcal{C}^2}$ are averaged (Cegielski, 2012, Theorem 2.2.21). Combined with the fact that F is α -cocoercive, the operator T is averaged (Davis & Yin, 2017, Proposition 2.1). The classic result of Krasnosel'skiĭ (Krasnosel'skiĭ, 1955) and Mann (Mann, 1953) asserts if, given any z^1 , a sequence $\{z^k\}$ is generated using updates of the form $z^{k+1} = T(z^k)$ for an averaged operator T , then $\{z^k\}$ converges to a fixed point $z^\circ \in \{z : T(z) = z\}$. Because the projection operator is 1-Lipschitz, it necessarily follows that $\{P_{\mathcal{C}^1}(z^k)\}$ converges to $P_{\mathcal{C}^1}(z^\circ)$. By Lemma B.1, we conclude $P_{\mathcal{C}^1}(z^\circ) \in \text{VI}(F(\cdot; d), \mathcal{C})$. \square

C. Constraint Decoupling

C.1. Minkowski Sum

This subsection provides a decoupling scheme for constraints structured as a Minkowski sum,¹¹ i.e.

$$\mathcal{C} \triangleq \mathcal{C}_1 + \dots + \mathcal{C}_K, \quad (32)$$

where $\mathcal{C}_k \subset \mathcal{X}$ and $\mathcal{C}_k = \mathcal{C}_k^1 \cap \mathcal{C}_k^2$ for all $k \in [K]$. The core idea is to avoid attempting to directly project onto \mathcal{C} and instead perform simple projections onto each set \mathcal{C}_k^i , assuming the projection onto \mathcal{C}_k^i admits an explicit formula. First, define the product space

$$\overline{\mathcal{X}} \triangleq \underbrace{\mathcal{X} \times \mathcal{X} \times \dots \times \mathcal{X}}_{K \text{ times}}. \quad (33)$$

For notational clarity, we denote elements of $\overline{\mathcal{X}}$ by overlines so each element $\overline{x} \in \overline{\mathcal{X}}$ is of the form $\overline{x} = (\overline{x}_1, \dots, \overline{x}_K)$ with $\overline{x}_k \in \mathcal{X}$ for all $k \in [K]$. Because \mathcal{X} is a Hilbert space, $\overline{\mathcal{X}}$ is naturally endowed with a scalar product $\langle \cdot, \cdot \rangle_{\overline{\mathcal{X}}}$ defined by

$$\langle \overline{x}, \overline{y} \rangle_{\overline{\mathcal{X}}} \triangleq \sum_{k=1}^K \langle \overline{x}_k, \overline{y}_k \rangle. \quad (34)$$

¹¹This arises in the modeling Wardrop equilibria in traffic routing problems.

Between \mathcal{X} and the product space $\overline{\mathcal{X}}$ we define two natural maps $Q^- : \overline{\mathcal{X}} \rightarrow \mathcal{X}$ and $Q^+ : \mathcal{X} \rightarrow \overline{\mathcal{X}}$ by

$$\begin{aligned} Q^-(\overline{x}) &\triangleq \sum_{k=1}^K \overline{x}_k, \\ Q^+(x) &\triangleq \underbrace{(x, x, \dots, x)}_{K \text{ copies}}. \end{aligned} \quad (35)$$

In words, $Q^-(\overline{x})$ maps down to \mathcal{X} by adding together the blocks of \overline{x} and $Q^+(x)$ maps up to $\overline{\mathcal{X}}$ by making K copies of x , thus motivating the use of “+” and “−” signs. Define the Cartesian product

$$\mathcal{A} \triangleq \mathcal{C}_1 \times \dots \times \mathcal{C}_K \subseteq \overline{\mathcal{X}}, \quad (36)$$

and note $Q^-(\mathcal{A}) = \mathcal{C}$. To further decouple each set \mathcal{C}_k , also define the Cartesian products

$$\mathcal{A}^i \triangleq \mathcal{C}_1^i \times \dots \times \mathcal{C}_K^i \quad \text{for all } i \in [2]. \quad (37)$$

so $\mathcal{A} = \mathcal{A}^1 \cap \mathcal{A}^2$. Note the projection onto \mathcal{A}^i can be computed component-wise; namely,

$$P_{\mathcal{A}^i}(\overline{x}) = \left(P_{\mathcal{C}_1^i}(\overline{x}_1), \dots, P_{\mathcal{C}_K^i}(\overline{x}_K) \right) \quad \text{for all } i \in [2]. \quad (38)$$

We now rephrase Algorithm 1, applied to a VI in the product space $\text{VI}(Q^+ \circ F \circ Q^-, \mathcal{A})$, into Algorithm 3 using \mathcal{A}^i in lieu of \mathcal{C}^i . The use of Algorithm 3 is justified by the following two lemmas. The first shows the product space operator is monotone whenever F is. The second shows the solution sets to the two VIs coincide, after applying Q^- to map down from $\overline{\mathcal{X}}$ to \mathcal{X} .

Lemma C.1. *If $F : \mathcal{X} \rightarrow \mathcal{X}$ is α -cocoercive, then $Q^+ \circ F \circ Q^-$ on $\overline{\mathcal{X}}$ is (α/K) -cocoercive.*

Proof. Fix any $\overline{x}, \overline{y} \in \overline{\mathcal{X}}$ and set $R_{\overline{x}} \triangleq (F \circ Q^-)(\overline{x})$ and $R_{\overline{y}} \triangleq (F \circ Q^-)(\overline{y})$. Then observe

$$\begin{aligned} &\langle Q^+(R_{\overline{x}}) - Q^+(R_{\overline{y}}), \overline{x} - \overline{y} \rangle_{\overline{\mathcal{X}}} \\ &= \sum_{k=1}^K \langle R_{\overline{x}} - R_{\overline{y}}, \overline{x}_k - \overline{y}_k \rangle \end{aligned} \quad (39a)$$

$$= \langle R_{\overline{x}} - R_{\overline{y}}, Q^-(\overline{x}) - Q^-(\overline{y}) \rangle. \quad (39b)$$

Substituting in the definition of $R_{\overline{x}}$ and $R_{\overline{y}}$ reveals

$$\begin{aligned} &\langle Q^+(R_{\overline{x}}) - Q^+(R_{\overline{y}}), \overline{x} - \overline{y} \rangle_{\overline{\mathcal{X}}} \\ &= \langle F(Q^-(\overline{x})) - F(Q^-(\overline{y})), Q^-(\overline{x}) - Q^-(\overline{y}) \rangle \end{aligned} \quad (40a)$$

$$\geq \alpha \|F(Q^-(\overline{x})) - F(Q^-(\overline{y}))\|^2 \quad (40b)$$

$$= \frac{\alpha}{K} \|Q^+ \circ F \circ Q^-(\overline{x}) - Q^+ \circ F \circ Q^-(\overline{y})\|_{\overline{\mathcal{X}}}^2, \quad (40c)$$

where the final equality follows from the definition of the norm on $\overline{\mathcal{X}}$. Because (40) holds for arbitrary $\overline{x}, \overline{y} \in \overline{\mathcal{X}}$, the result follows. \square

Proposition C.2. For $F: \mathcal{X} \rightarrow \mathcal{X}$, $\bar{x}^\circ \in \text{VI}(Q^+ \circ F \circ Q^-, \mathcal{A})$ if and only if $Q^-(\bar{x}^\circ) \in \text{VI}(F, \mathcal{C})$.

Proof. Fix $\bar{y} \in \mathcal{A}$ and $\bar{x}^\circ \in \text{VI}(Q^+ \circ F \circ Q^-, \mathcal{A})$. Similarly to the proof of Lemma C.1, observe

$$\begin{aligned} & \langle (Q^+ \circ F \circ Q^-)(\bar{x}^\circ), \bar{y} - \bar{x}^\circ \rangle_{\bar{\mathcal{X}}} \\ &= \sum_{k=1}^K \langle (F \circ Q^-)(\bar{x}^\circ), \bar{y}_k - \bar{x}_k^\circ \rangle \end{aligned} \quad (41a)$$

$$= \langle F(Q^-(\bar{x}^\circ)), Q^-(\bar{y}) - Q^-(\bar{x}^\circ) \rangle. \quad (41b)$$

Because $Q^-(\mathcal{A}) = \mathcal{C}$, it follows that $x^\circ \triangleq Q^-(\bar{x}^\circ) \in \mathcal{C}$ and $w \triangleq Q^-(\bar{y}) \in \mathcal{C}$. Consequently,

$$\begin{aligned} 0 &\leq \langle (Q^+ \circ F \circ Q^-)(\bar{x}^\circ), \bar{y} - \bar{x}^\circ \rangle_{\bar{\mathcal{X}}} \\ &= \langle F(x^\circ), w - x^\circ \rangle. \end{aligned} \quad (42)$$

Because \bar{y} was arbitrarily chosen, (42) holds for all $w \in \mathcal{C}$ and, thus, $Q^-(\bar{x}^\circ) \in \text{VI}(F, \mathcal{C})$.

Conversely, fix $\bar{y} \in \mathcal{A}$ and $\bar{x}^\circ \in \bar{\mathcal{X}}$ such that $Q^-(\bar{x}^\circ) \in \text{VI}(F, \mathcal{C})$. Then $Q^-(\bar{y}) \in \mathcal{C}$ and

$$0 \leq \langle F(Q^-(\bar{x}^\circ)), Q^-(\bar{y}) - Q^-(\bar{x}^\circ) \rangle \quad (43a)$$

$$= \sum_{k=1}^K \langle F(Q^-(\bar{x}^\circ)), \bar{y}_k - \bar{x}_k^\circ \rangle \quad (43b)$$

$$= \langle (Q^+ \circ F \circ Q^-)(\bar{x}^\circ), \bar{y} - \bar{x}^\circ \rangle_{\bar{\mathcal{X}}}. \quad (43c)$$

Together the inequality (43) and the fact $\bar{y} \in \mathcal{A}$ was arbitrarily chosen imply $\bar{x}^\circ \in \text{VI}(Q^+ \circ F \circ Q^-, \mathcal{A})$. This completes the proof. \square

C.2. Intersections of Constraints

For completeness, we also consider constraints \mathcal{C} that may be expressed as the intersection of several sets, *i.e.* $\mathcal{C} = \mathcal{C}_1 \cap \mathcal{C}_2 \cdots \cap \mathcal{C}_K$. Let $\bar{\mathcal{X}}$, $\langle \cdot, \cdot \rangle_{\bar{\mathcal{X}}}$, Q^+ and Q^- be as in Appendix C.1. Next define¹²

$$\begin{aligned} \mathcal{B}^1 &\triangleq \mathcal{C}_1 \times \cdots \times \mathcal{C}_K, \\ \mathcal{B}^2 &\triangleq Q^+(\mathcal{X}) = \{\bar{x} \in \bar{\mathcal{X}} : x_1 = \cdots = x_K\}, \\ \mathcal{B} &\triangleq \mathcal{B}^1 \cap \mathcal{B}^2, \end{aligned} \quad (44)$$

Note $Q^-(\mathcal{B}) = \mathcal{C}$. The logic is now the same as before; rephrase Algorithm 1 using \mathcal{B}^i in place of \mathcal{C}^i . The projection $P_{\mathcal{B}^1}$ can be computed component-wise via

$$P_{\mathcal{B}^1}(\bar{x}) = (P_{\mathcal{C}_1}(\bar{x}_1), \dots, P_{\mathcal{C}_K}(\bar{x}_K)), \quad (45)$$

and $P_{\mathcal{B}^2}(\bar{x})$ has a simple closed form given in the following lemma.

¹²Note \mathcal{A} in Appendix C.1 is the same as \mathcal{B}^1 in (44), *i.e.* $\mathcal{B}^1 = \mathcal{A}$.

Lemma C.3. With notation as above, $P_{\mathcal{B}^2}(\bar{x}) = Q^+\left(\frac{1}{K} \sum_{k=1}^K \bar{x}_k\right)$.

Proof. By the definition of a projection and the norm on $\bar{\mathcal{X}}$,

$$P_{\mathcal{B}^2}(\bar{x}) \triangleq \operatorname{argmin}_{\bar{z} \in \mathcal{B}^2} \|\bar{z} - \bar{x}\|_{\bar{\mathcal{X}}}^2 \quad (46a)$$

$$= \operatorname{argmin}_{\bar{z} \in \mathcal{B}^2} \sum_{k=1}^K \|\bar{z}_k - \bar{x}_k\|^2 \quad (46b)$$

$$= Q^+(z^\#), \quad (46c)$$

where $z^\# = \operatorname{argmin}_{z \in \mathcal{X}} \sum_{k=1}^K \|z - \bar{x}_k\|^2$, so $z^\#$ satisfies the following optimality condition

$$\begin{aligned} 0 &= \frac{d}{dz} \left[\sum_{k=1}^K \|z - \bar{x}_k\|^2 \right]_{z=z^\#} \\ &= \sum_{k=1}^K 2(z^\# - \bar{x}_k) \\ &= 2K \left(z^\# - \frac{1}{K} \sum_{k=1}^K \bar{x}_k \right). \end{aligned}$$

This implies

$$z^\# = \frac{1}{K} \sum_{k=1}^K \bar{x}_k. \quad (47)$$

Together (46) and (47) yield the result, completing the proof. \square

For each operator $F: \mathcal{X} \rightarrow \mathcal{X}$, we define a corresponding product space operator $\bar{F}: \bar{\mathcal{X}} \rightarrow \bar{\mathcal{X}}$ via

$$\bar{F}(\bar{x}) \triangleq (F(\bar{x}_1), \dots, F(\bar{x}_K)). \quad (48)$$

This definition enables us to show a direct equivalence between a VI in the original space \mathcal{X} and the product space $\bar{\mathcal{X}}$. That is, we complete the analysis in the following lemmas by showing the solution set of an appropriate VI in the product space coincides with that of the original VI.

Proposition C.4. If $F: \mathcal{X} \rightarrow \mathcal{X}$ is α -cocoercive, then the operator $\bar{F}: \bar{\mathcal{X}} \rightarrow \bar{\mathcal{X}}$ is α -cocoercive.

Proof. Fix any $\bar{x}, \bar{y} \in \bar{\mathcal{X}}$. Then observe

$$\begin{aligned} & \langle \bar{F}(\bar{x}) - \bar{F}(\bar{y}), \bar{x} - \bar{y} \rangle_{\bar{\mathcal{X}}} \\ &= \sum_{k=1}^K \langle F(\bar{x}_k) - F(\bar{y}_k), \bar{x}_k - \bar{y}_k \rangle \end{aligned} \quad (49a)$$

$$\geq \alpha \sum_{k=1}^K \|F(\bar{x}_k) - F(\bar{y}_k)\|^2 \quad (49b)$$

$$= \alpha \|\bar{F}(\bar{x}) - \bar{F}(\bar{y})\|_{\bar{\mathcal{X}}}^2. \quad (49c)$$

Algorithm 3 Nash Fixed Point Network (Minkowski Sum Constraints $\mathcal{C} = \mathcal{C}_1 + \dots + \mathcal{C}_K$)

1: $\mathcal{N}_\Theta(d)$:	\triangleleft Input data is d
2: $n \leftarrow 1$	\triangleleft Initialize counter
3: for $k = 1, 2, \dots, K$	
4: $\bar{z}_k^1 \leftarrow \hat{z}$	\triangleleft Initialize iterates to $\hat{z} \in \mathcal{X}$
5: while $\sum_{k=1}^K \ \bar{z}_k^n - \bar{z}_k^{n-1}\ > \varepsilon$ or $n = 1$	\triangleleft Loop until convergence at fixed point
6: for $k = 1, 2, \dots, K$	\triangleleft Loop over constraints \mathcal{C}_k^1
7: $\bar{x}_k^{n+1} \leftarrow P_{\mathcal{C}_k^1}(\bar{z}_k^n)$	\triangleleft Project onto constraint set
8: $v^{n+1} \leftarrow \sum_{k=1}^K \bar{x}_k^{n+1}$	\triangleleft Combine projections
9: for $k = 1, 2, \dots, K$	\triangleleft Loop over constraints \mathcal{C}_k^2
10: $\bar{y}_k^{n+1} \leftarrow P_{\mathcal{C}_k^2}(2\bar{x}_k^{n+1} - \bar{z}_k^n - \alpha F_\Theta(v^{n+1}; d))$	\triangleleft Block-wise project reflected gradients
11: $\bar{z}_k^{n+1} \leftarrow \bar{z}_k^n - \bar{x}_k^{n+1} + \bar{y}_k^{n+1}$	\triangleleft Apply block-wise updates
12: $n \leftarrow n + 1$	\triangleleft Increment counter
13: return v^n	\triangleleft Output inference

Algorithm 4 Nash Fixed Point Network (Intersection Constraints $\mathcal{C} = \mathcal{C}_1 \cap \dots \cap \mathcal{C}_K$)

1: $\mathcal{N}_\Theta(d)$:	\triangleleft Input data is d
2: $n \leftarrow 1$	\triangleleft Initialize counter
3: for $k = 1, 2, \dots, K$	
4: $\bar{z}_k^1 \leftarrow \hat{z}$	\triangleleft Initialize iterates to $\hat{z} \in \mathcal{X}$
5: while $\sum_{k=1}^K \ \bar{z}_k^n - \bar{z}_k^{n-1}\ > \varepsilon$ or $n = 1$	\triangleleft Loop until convergence at fixed point
6: for $k = 1, 2, \dots, K$	
7: $\bar{x}_k^{n+1} \leftarrow P_{\mathcal{C}_k}(\bar{z}_k^n)$	\triangleleft Project \bar{x}^n onto \mathcal{B}^1
8: $v^{n+1} \leftarrow \frac{1}{K} \sum_{k=1}^K (2\bar{x}_k^{n+1} - \bar{z}_k^n - \alpha F_\Theta(\bar{x}_k^{n+1}; d))$	\triangleleft Project reflected gradient onto \mathcal{B}^2
9: for $k = 1, 2, \dots, K$	\triangleleft to obtain $\bar{y}^{n+1} = Q^+(v^{n+1})$
10: $\bar{z}_k^{n+1} \leftarrow \bar{z}_k^n - \bar{x}_k^{n+1} + v^{n+1}$	\triangleleft Combine auxiliary sequences
11: $n \leftarrow n + 1$	\triangleleft Increment counter
12: return \bar{x}_1^n	\triangleleft Output inference

Because (49) holds for arbitrarily chosen $\bar{x}, \bar{y} \in \bar{\mathcal{X}}$, we conclude \bar{F} is α -cocoercive. \square

Lemma C.5. For α -cocoercive $F: \mathcal{X} \rightarrow \mathcal{X}$, $x^\circ \in \text{VI}(F, \mathcal{C})$ if and only if $Q^+(x^\circ) \in \text{VI}(\bar{F}, \mathcal{B})$.

Proof. Fix any $x^\circ \in \text{VI}(F, \mathcal{C})$ and set $\bar{x}^\circ = Q^+(x^\circ)$. An elementary proof shows $Q^+ : \mathcal{C} \rightarrow \mathcal{B}$ is a bijection. Together

with the fact x° is a VI solution, this implies

$$0 \leq K \langle F(x^\circ), y - x^\circ \rangle, \text{ for all } y \in \mathcal{C}$$

$$\iff 0 \leq \sum_{k=1}^K \langle F(x^\circ), \bar{y}_k - x^\circ \rangle, \text{ for all } \bar{y} \in \mathcal{B} \quad (50a)$$

$$\iff 0 \leq \sum_{k=1}^K \langle F(\bar{x}_k^\circ), \bar{y}_k - \bar{x}_k^\circ \rangle, \text{ for all } \bar{y} \in \mathcal{B} \quad (50b)$$

$$\iff 0 \leq \langle \bar{F}(\bar{x}^\circ), \bar{y} - \bar{x}^\circ \rangle_{\bar{\mathcal{X}}}, \text{ for all } \bar{y} \in \mathcal{B}. \quad (50c)$$

By the transitive property, the first and final expressions in (50) are equivalent, and we are done. \square

C.3. Projections onto Intersections of Hyperplanes

Consider the set $\mathcal{C} \triangleq \{x : Nx = b\} \subseteq \mathcal{X}$, and note \mathcal{C} is closed and convex so the projection operator onto \mathcal{C} is well-defined and given by

$$\begin{aligned} P_{\mathcal{C}}(z) &= \operatorname{argmin}_{x \in \mathcal{C}} \frac{1}{2} \|x - z\|^2 \\ &= \operatorname{argmin}_{x \in \mathcal{X}} \frac{1}{2} \|x - z\|^2 \text{ s.t. } Nx = b. \end{aligned} \quad (51)$$

For completeness we express (and prove) a projection formula for \mathcal{C} via the following lemma.

Lemma C.6. *For nonempty $\mathcal{C} \triangleq \{x : Nx = b\}$, the projection $P_{\mathcal{C}}$ is given by*

$$P_{\mathcal{C}}(z) = z - N^\dagger(Nz - b), \quad (52)$$

where $N^\dagger \triangleq U\Sigma^{-1}V^\top$ and $U\Sigma V$ is the compact singular value decomposition of N such that U and V have orthonormal columns and Σ is invertible.

Proof. Referring to (51), we see the associated Lagrangian is given by

$$\mathcal{L}(x, \lambda) \triangleq \frac{1}{2} \|x - z\|^2 + \langle \lambda, Nx - b \rangle. \quad (53)$$

The optimizer $x^\# \triangleq P_{\mathcal{C}}(z)$ satisfies the optimality condition $0 = \nabla \mathcal{L}(x^\#, \lambda^\#)$ for some $\lambda^\#$, which can be expanded as

$$\begin{aligned} 0 &= \nabla_x \left[\mathcal{L}(x, \lambda) \right]_{(x, \lambda) = (x^\#, \lambda^\#)} \\ &= x^\# - z + N^\top \lambda^\#, \end{aligned} \quad (54a)$$

$$\begin{aligned} 0 &= \nabla_\lambda \left[\mathcal{L}(x, \lambda) \right]_{(x, \lambda) = (x^\#, \lambda^\#)} \\ &= Nx^\# - b. \end{aligned} \quad (54b)$$

We claim it suffices to choose

$$\lambda^\# = (U\Sigma^{-2}U^\top)(Nz - b). \quad (55)$$

By (54a), this choice yields

$$x^\# = z - N^\top \lambda^\# \quad (56a)$$

$$= z - N^\top (U\Sigma^{-2}U^\top)(Nz - b) \quad (56b)$$

$$= z - (V\Sigma U^\top)(U\Sigma^{-2}U^\top)(Nz - b) \quad (56c)$$

$$= z - (V\Sigma^{-1}U^\top)(Nz - b) \quad (56d)$$

$$= z - N^\dagger(Nz - b). \quad (56e)$$

To prove this formula for $x^\#$ gives the projection, it suffices to show the remaining condition $Nx^\# = b$ is satisfied. Decomposing N into its singular value decomposition, observe

$$Nx^\# = N(z - (V\Sigma^{-1}U^\top)(Nz - b)) \quad (57a)$$

$$= Nz - (U\Sigma V^\top)(V\Sigma^{-1}U^\top)(Nz - b) \quad (57b)$$

$$= Nz - (U\Sigma V^\top)(V\Sigma^{-1}U^\top)(U\Sigma V^\top z - b) \quad (57c)$$

$$= Nz - U\Sigma V^\top z + UU^\top b \quad (57d)$$

$$= UU^\top b. \quad (57e)$$

The range of N is contained in the subspace spanned by the orthonormal columns of U , i.e. $\operatorname{range}(N) \subseteq \operatorname{span}(u^1, \dots, u^r)$, where u^i is the i -th column of U and r is the rank of N . Because \mathcal{C} is nonempty, $b \in \operatorname{range}(N)$ and it follows that there exists scalars $\alpha_1, \dots, \alpha_r$ such that

$$b = \sum_{i=1}^r \alpha_i u^i. \quad (58)$$

Through direct substitution, we deduce

$$\begin{aligned} UU^\top b &= UU^\top \sum_{i=1}^r \alpha_i u^i \\ &= U \left(\sum_{i,j=1}^r \alpha_i \langle u^j, u^i \rangle \right) \\ &= U \sum_{i=1}^r \alpha_i e^i \\ &= \sum_{i=1}^r \alpha_i u^i \\ &= b. \end{aligned} \quad (59)$$

Thus, (57) and (59) together show the final optimality condition is satisfied, proving the claim. \square

Remark C.7. In our traffic routing experiments, we use the built-in SVD function in Pytorch, threshold the tiny singular values to be zero, and invert the remaining entries.

D. Experimental Supplementary Material

D.1. Matrix Games

Our Payoff-Net architecture is based upon the architecture described in (Ling et al., 2018)¹³, but we make several modifications, which we now describe. First, we update their implementation of a differentiable game solver so as to be compatible with the current Pytorch autograd syntax. Second, we modify their code to enable Payoff-Net to handle matrix games of arbitrary size (not just 3 dimensional action

¹³and downloaded from https://github.com/lingchun kai/payoff_learning

sets). Finally, we use two, instead of one, fully connected layers with ReLU activation to map context d to payoff matrix P , which is then provided to the differentiable game solver. If a is as in Section 5.1 then Payoff-Net has $9 + \frac{3}{2}(a^2 - a)$ tunable parameters.

The N-FPN architecture is as described in Algorithm 2 with F_Θ consisting of two fully connected. More specifically,

$$F_\Theta(x; d) = x + W_2(x + \sigma(W_1 d))$$

where W_1 and W_2 are matrices of tunable parameters. Each N-FPN has $6a + 4a^2$ tunable parameters.

For training both networks we use Adam with starting step-size 10^{-3} and a scheduler that halves the step-size when the decrease in test loss is determined to plateau. All code is available in the supplementary materials.

D.2. Incidence Matrix

For a directed graph with vertices V and arcs E the vertex-arc incidence matrix $N \in \mathbb{R}^{|V| \times |E|}$ is defined by

$$N_{ij} \triangleq \begin{cases} +1 & \text{if } (i, j) \in E \\ -1 & \text{if } (j, i) \in E \\ 0 & \text{otherwise} \end{cases} \quad (60)$$

For example, for the simple road network shown in Figure 4 the incidence matrix is

$$N = \begin{bmatrix} -1 & 0 & -1 & 0 & 0 \\ 0 & 0 & 1 & -1 & -1 \\ 1 & -1 & 0 & 1 & 0 \\ 0 & 1 & 0 & 0 & 1 \end{bmatrix}. \quad (61)$$

D.3. Toy Traffic Routing Model

We consider the traffic network shown in Figure 4 (with incidence matrix given in (61)) and a single OD pair: $(v_1, v_4, 1)$. We use the contextual travel-time functions¹⁴

$$t_e(x_e; d) \triangleq f_e \cdot \left(1 + \left[\frac{x_e}{c(d)_e}\right]^4\right), \quad (62)$$

where $f = (1, 2, \sqrt{2}, \sqrt{3}, 1)$ and

$$c(d) \triangleq \tilde{c} \odot (1 + P_{[-\epsilon, \epsilon]}(Wd)), \quad (63)$$

for $\epsilon = 0.4$ and $\tilde{c} = (0.4, 0.8, 0.8, 0.6, 0.3)$, and \odot denoting element-wise (*i.e.* Hadamard) product. The matrix W is constructed by sampling the entries of the first column uniformly and i.i.d. on $(-10, 0]$, and sampling the entries of the remaining columns uniformly and i.i.d. on $[0, 1)$. This form of W implies that $d_1 > 0$ decreases the capacity of each

road segment, albeit by varying amounts. Thus d_1 could be interpreted as, for example, inches of rainfall. We use this interpretation to generate Figures 1 and 4; taking any d with d_1 large corresponds to a rainy day while if d_1 small it can be interpreted as a sunny day. We generate training data by sampling d i.i.d. and uniformly from $[0, 0.25]^5$ and then solving for $x_d^* \in \text{VI}(F, \mathcal{C})$ using Algorithm 1 with

$$\begin{aligned} F(x; d) &\triangleq [t_1(x_1; d), \dots, t_5(x_5; d)]^\top, \\ \mathcal{C}^1 &\triangleq \{x : Nx = b\}, \\ b &\triangleq [-1, 0, 0, 1, 0]^\top, \\ \mathcal{C}^2 &= \mathbb{R}_{\geq 0}^5 \end{aligned} \quad (64)$$

The projection onto \mathcal{C}^2 is given by a component-wise ReLU and the projection onto \mathcal{C}^1 is given in Appendix C.3.

D.4. Real-World Traffic Routing Model

Similarly to Appendix D.3, we consider a traffic network for the real data described in Table 2. For each dataset, we obtain the OD pairs b_k , the free-flow time f_e , the incidence matrix N , and the capacity values \tilde{c} on each edge from the Transportation Networks website ([tra](#)). To generate the data, we use the contextual travel-time function

$$t_e(x_e; d) \triangleq f_e \cdot \left(1 + 0.5 \left[\frac{x_e}{c(d)_e}\right]^4\right), \quad (65)$$

where we contextualize the capacities with

$$c(d) \triangleq \tilde{c} \odot (1 + P_{[-\epsilon, \epsilon]}(Wd)). \quad (66)$$

Here, we set $\epsilon = 0.8$ for the Anaheim dataset and $\epsilon = 0.3$ for the remaining four datasets. We choose ϵ for the Anaheim dataset as we found the resulting actions x_d^* were too similar for $\epsilon = 0.3$ (making it too easy to train an operator fitting this dataset). Similarly to the toy traffic problem, the matrix W is constructed by sampling the entries of the first column uniformly and i.i.d. on $(-10, 0]$, and sampling the entries of the remaining columns uniformly and i.i.d. on $[0, 1)$. Since we have multiple OD pairs, the constraints are given by the Minkowski sum of polyhedral sets. Thus, we generate the 5500 training data pairs (d, x_d^*) using Algorithm 3.

D.5. Network Architecture for Traffic Routing

We describe the architectures used to generate Table 2. We use fully-connected layers to parameterize F_θ . We have an opening layer, which maps from context (in our experiments, the context dimension is 10) to a 100-dimensional latent space. In the latent space, we use either one or two hidden layers (depending on the dataset) with 100-dimensional inputs and outputs. The last layer maps from the hidden dimension to the action space, *i.e.*, number of edges. Since

¹⁴The form of this function is motivated by the well-known Bureau of Public Roads (BPR) function

the number of edges vary per dataset, the number of tunable parameters also vary. Finally, we use a maximum depth of 50 iterations in our N-FPN architecture with a stopping tolerance of $\epsilon = 10^{-4}$.

D.6. Training Details

As described in Section 5.2, we generate 5000 training samples and 500 testing samples for all datasets. For all datasets, we use batch size of 500 and Adam (Kingma & Ba, 2015) with constant learning rates and 200 epochs. The learning rates are chosen to be 5×10^{-5} for Berlin-Tiergarten and 10^{-3} for the remaining datasets. All networks are trained using Google Colaboratory (Bisong, 2019).

E. Data Provenance

For the Rock, Paper, Scissors experiment, we generated our own data following the experimental set-up described in (Ling et al., 2018). For the toy traffic routing problem, we also our own data, using the same traffic network as (Li et al., 2020) but modifying their experiment so as to make road capacities contextual. The Sioux Falls, Berlin-Tiergarten and Berlin Friedrichshain and Eastern Massachusetts datasets are from (LeBlanc et al., 1975; Jahn et al., 2005) and (Zhang et al., 2016) respectively. The Anaheim dataset was provided by Jeff Ban and Ray Jayakrishnan and was originally hosted at <https://www.bgu.ac.il/~bargera/tntp/>. All datasets were downloaded from (tra) and are used under the “academic use only” license described therein.

F. Additional Plots

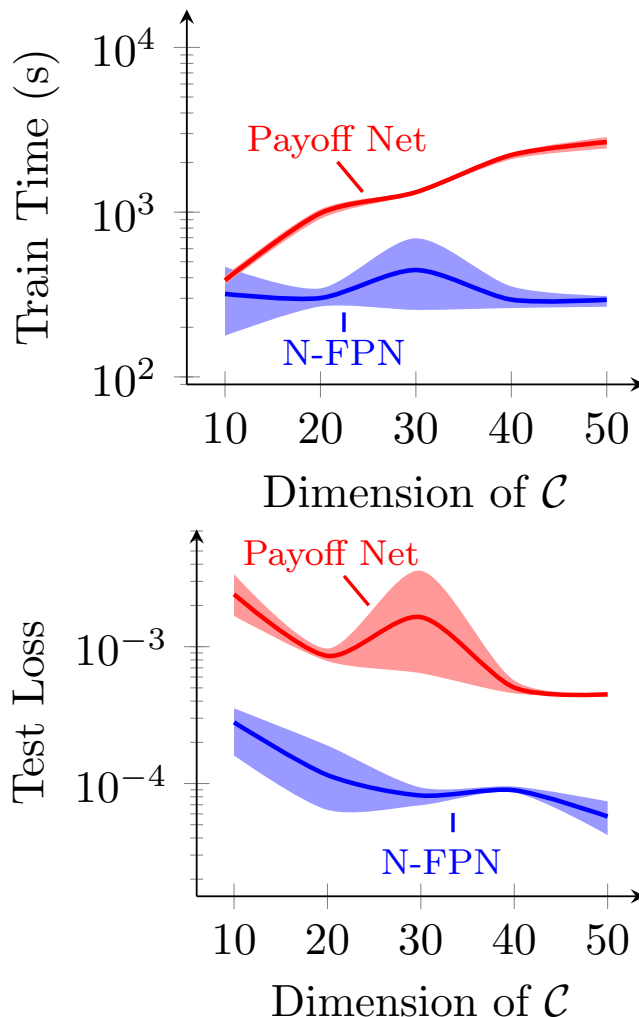


Figure 6. Total training time (left) and final test loss (center) for Nash-FPN and Payoff-Net for matrix games of increasing size a , trained for 100 epochs or until a test loss less than 10^{-5} is achieved. Here, we omit the results for N-FPN with $\dim(\mathcal{C}) = 100, 150$ and 200 (see Figure 2) for ease of comparison.

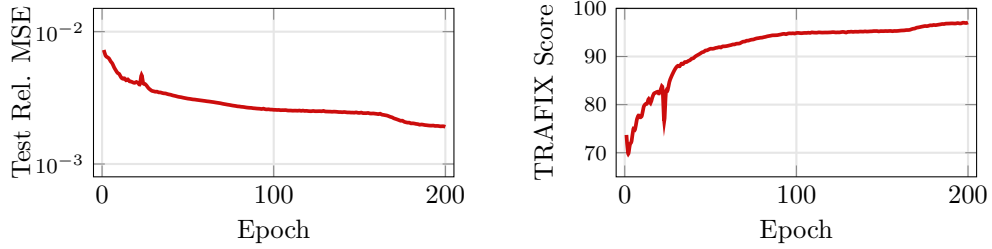


Figure 7. Plots for N-FPN performance on Sioux Falls testing data. The left plot shows convergence of expected mean squared error on testing data after each training epoch and the right shows the expected TRAFIX score on testing data after each training epoch.

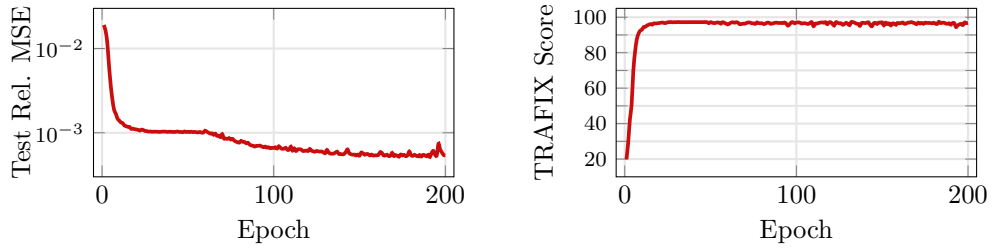


Figure 8. Plots for N-FPN performance on Berlin Friedrichshain testing data. The left plot shows convergence of expected relative mean squared error on testing data after each training epoch and the right shows the expected TRAFIX score on testing data after each training epoch.

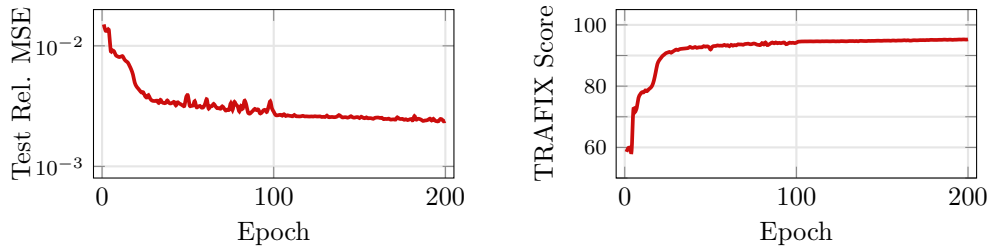


Figure 9. Plots for N-FPN performance on Anaheim testing data. The left plot shows convergence of expected relative mean squared error on testing data after each training epoch and the right shows the expected TRAFIX score on testing data after each training epoch.

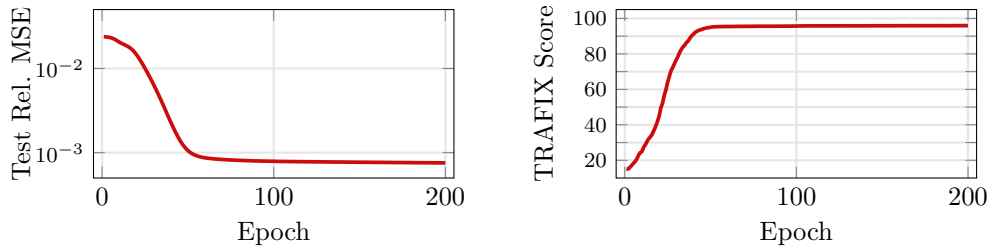


Figure 10. Plots for N-FPN performance on Berlin Tiergarten testing data. The left plot shows convergence of expected relative mean squared error on testing data after each training epoch and the right shows the expected TRAFIX score on testing data after each training epoch.